AGU PUBLICATIONS

Geochemistry, Geophysics, Geosystems

RESEARCH ARTICLE
10.1002/2014GC005414

Key Points:
- Two styles of edge-driven convection are recognized
- Edge-driven convection with asthenospheric shear produces localized thinning
- Volcanism in Atlas mountains explained by numerical models of EDC

Supporting Information:
- Readme
- Detailed Methods

Correspondence to:
L. Kaislaniemi,
lars.kaislaniemi@iki.fi

Citation:
Kaislaniemi, L., and J. van Hunen (2014), Dynamics of lithospheric thinning and mantle melting by edge-driven convection: Application to Moroccan Atlas mountains, *Geochem. Geophys. Geosyst.*, *15*, 3175–3189, doi:10.1002/2014GC005414.

Received 12 MAY 2014
Accepted 13 JUL 2014
Accepted article online 16 JUL 2014
Published online 19 AUG 2014

Dynamics of lithospheric thinning and mantle melting by edge-driven convection: Application to Moroccan Atlas mountains

Lars Kaislaniemi[1] and Jeroen van Hunen[1]

[1]Department of Earth Sciences, Durham University, Durham, UK

Abstract Edge-driven convection (EDC) forms in the upper mantle at locations of lithosphere thickness gradients, e.g., craton edges. In this study we show how the traditional style of EDC, a convection cell governed by the cold downwelling below an edge alternates with another style of EDC, in which the convection cell forms as a secondary feature with a hot asthenospheric shear flow from underneath the thicker lithosphere. These alternating EDC styles produce episodic lithosphere erosion and decompression melting. Three-dimensional models of EDC show that convection rolls form perpendicular to the thickness gradient at the lithosphere-asthenosphere boundary. Stagnant-lid convection scaling laws are used to gain further insight in the underlying physical processes. Application of our models to the Moroccan Atlas mountains region shows that the combination of these two styles of EDC can reproduce many of the observations from the Atlas mountains, including two distinct periods of Cenozoic volcanism, a semicontinuous corridor of thinned lithosphere under the Atlas mountains, and piecewise delamination of the lithosphere. A very good match between observations and numerical models is found for the lithosphere thicknesses across the study area, amounts of melts produced, and the length of the quiet gap in between volcanic episodes show quantitative match to observations.

1. Introduction

Edge-driven convection (EDC) is a term coined for convection patterns forming at locations of significant lithosphere thickness gradients, e.g., craton edges. First described as a craton edge flow instability by *Elder* [1976] in his laboratory experiments, EDC has since been studied by numerical experiments [e.g., *King and Anderson*, 1995, 1998]. Two styles of EDC can be distinguished, termed here as EDC *sensu stricto* (EDC s.s.) and EDC with shear (EDC w.s.). EDC s.s. is dominated by cold downward flow caused by the relatively cold sloping boundary (the edge) of the thicker lithosphere cooling the sublithospheric mantle next to it (Figure 1a). EDC w.s. is caused by horizontal flow from below the thicker lithosphere to the direction of the thinner lithosphere, as a consequence of a long wavelength horizontal temperature difference between the mantle underneath the thicker lithosphere and the thinner lithosphere. The shear caused by this large scale flow induces a small secondary convection cell in the corner between the thicker and thinner lithospheres (Figure 1b).

The upward flow, inherently present in both styles of EDC, is a potential cause for decompression mantle melting and dynamic topography effects. Consequently, EDC has been proposed in many locations where there is a clear lithosphere gradient present. For example, EDC has been suggested to be the cause for the African and South American intraplate volcanism [*King*, 2000], the high topography and volcanism surrounding the Colorado plateau in southwestern United States [*van Wijk et al*., 2010], the seismic structure of the mantle and increased heat flow in the Canadian Cordillera [*Hardebol et al*., 2012], and the alternating low-high-low topography of the Bermuda Rise in the western Atlantic [*Shahnas and Russell*, 2004]. Generally, EDC can be expected to be present where two lithospheric domains of different thicknesses meet. These thicknesses often reflect the different tectonothermal ages of the lithospheric terranes, and, for convenience, we shall refer to these domains as *protons* and *tectons* [*Griffin et al*., 2003; *Janse*, 1994], where proton refers to the thicker, more viscous, lithosphere being older than Neoproterozoic in age, and tecton refers to the thinner lithosphere.

The inherent differences between the two styles of EDC (Figure 1) have been given little attention, and many studies either assume EDC s.s. or do not explicitly mention which style of EDC they have intended to

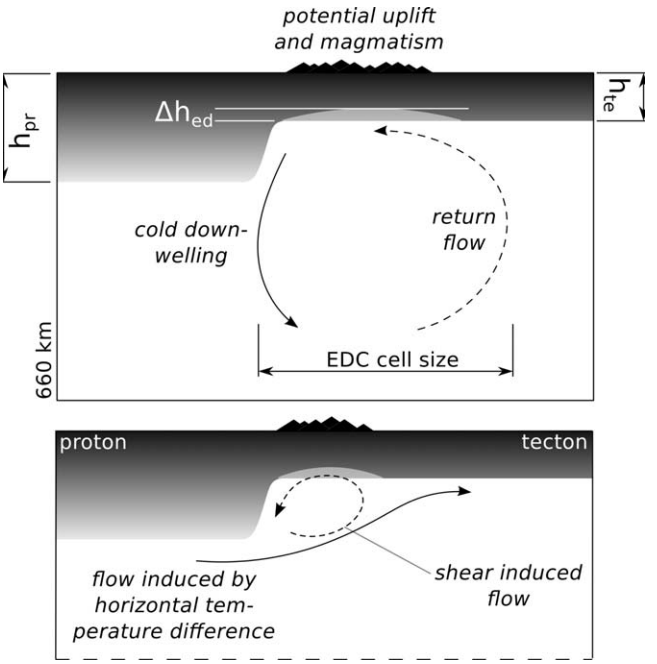

Figure 1. Two styles of edge-driven convection. (a) EDC *sensu stricto*, where the boundary of the cold thick lithosphere on the left (the proton or archon) cools down the asthenosphere next to it. This leads to downwellings at the edge and a return flow further away underneath the thinner lithosphere (or tecton) on the right. (b) EDC with shear, where the higher than horizontal average temperature below the proton leads to horizontal mantle flow to underneath the tecton, and causes a small convection cell to form next to the edge.

study. As noted by *King and Anderson* [1998], EDC s.s. is very sensitive to long wavelength mantle temperature perturbations and there seems to be a continuum from EDC s.s. to EDC w.s.: if the temperature difference between sublithospheric mantles of the proton and tecton exceeds 0.1 to 1 %, the EDC s.s. is overruled by the large scale flow and can even switch to EDC w.s. The difference in sublithospheric mantle temperatures could be caused by large-scale mantle flow patterns (e.g., mantle plumes), and can also be triggered by the thermal insulating effect of the thick lithosphere above [e.g., *Gurnis*, 1988].

Additionally, EDC s.s. is sensitive to relative velocity of the lithosphere and the asthenosphere. Plate movements, relative to the asthenosphere below, exceeding 1 cm/yr can suppress the EDC s.s. [*King and Anderson*, 1998], and, depending on the direction of the plate movement relative to the thickness gradient, cause convection similar to EDC w.s., also referred to as shear-driven upwelling [*Conrad et al*., 2010].

The convection cell caused by EDC s.s. dominates a large portion of the upper mantle height (∼300–500 km diameter) [e.g., *van Wijk et al*., 2010; *King*, 2000]. Much smaller convection cell sizes are observed in the case of EDC w.s., usually in the order of 150–200 km, as shown by *King and Anderson* [1998]. In this respect, EDC s.s. is a viable mechanism to explain observations spanning many hundreds of kilometers in horizontal direction, e.g., the aforementioned high topography of the Western Atlantic, spanning over 1000 km in width [*Shahnas and Russell*, 2004]. However, due to its large convection cell size, EDC s.s. (in the sense of *King and Anderson* [1995]) is hardly able to produce very local effects, such as those observed in NW African Atlas mountains in Morocco: Here intraplate orogeny close to the West African craton edge is associated with Cenozoic volcanism and localized strong thinning of the lithosphere along the craton edge. *Missenard and Cadoux* [2012] were first to suggest the existence of EDC under the Atlas mountains. Due to strong lithospheric thickness gradient in this area, it is an ideal location for an EDC to take place. As the thinned, narrow lithospheric corridor is very close to the craton edge, it is more probably caused by the EDC w.s. rather than EDC s.s.

We have studied the features of combined EDC w.s. and EDC s.s. using numerical models and applied those to the Moroccan Atlas mountains to test the hypothesis of EDC in this area.

1.1. Cenozoic Volcanism in the Moroccan Atlas Mountains

The Moroccan Atlas mountains (High and Middle Atlas) are an intraplate orogeny, uplifted in the Cenozoic by combination of lithospheric thinning and crustal shortening [*Missenard et al*., 2006]. They are formed as tectonically inverted basins, deformed along the inherited zones of weaknesses that were created during the opening of the Atlantic ocean in the late Triassic to early Jurassic [*Frizon de Lamotte et al*., 2000, and references therein]. The amount of shortening in Atlas mountains is modest (15–30% for the High Atlas and 10 % for the Middle Atlas) [*Beauchamp et al*., 1999; *Teixell et al*., 2003; *Gomez et al*., 1998; *Teixell et al*., 2009] and it has been suggested that lithospheric thinning is responsible for one third of the elevation in western

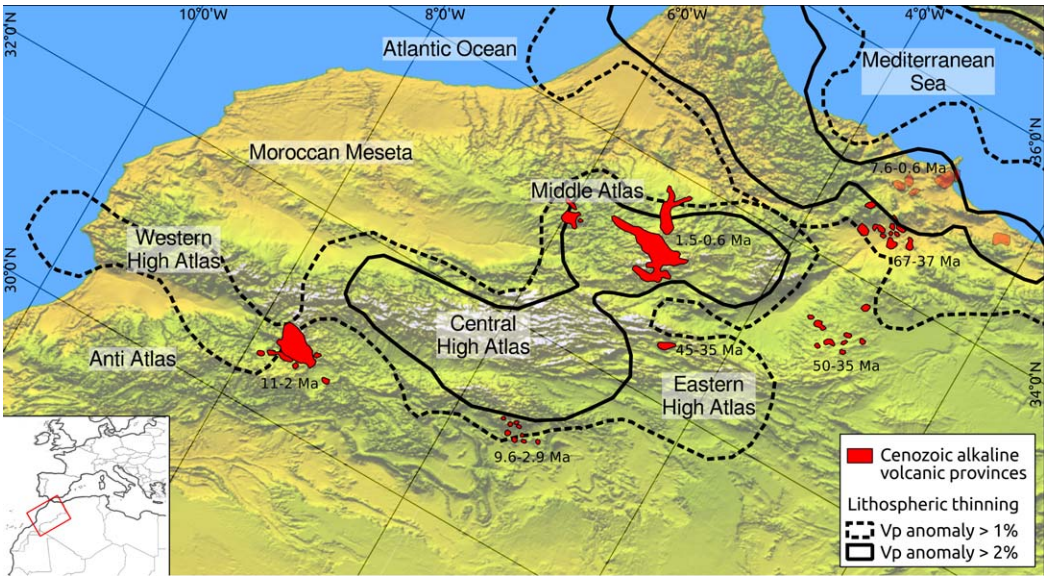

Figure 2. The topography of the Moroccan Atlas mountains (background map, NASA Shuttle Radar Topography Mission [*Farr et al*., 2007]) overlaid by the Cenozoic alkaline volcanic provinces (in red, from *Missenard and Cadoux* [2012]). The three volcanic provinces in the North (transparent color) have transitional calc-alkaline to alkaline chemical affinity and are partly related to the Rif subduction system. Black contour lines delineate the area of thinned lithosphere, where Vp velocities at 50 km depth are slower by 1% (dashed line) or 2 % (solid line) [from *Bezada et al*., 2014].

high Atlas, most of the elevation in Anti-Atlas, and about half of the elevation in the central High Atlas and middle Atlas [*Missenard et al*., 2006, see also *Miller and Becker*, 2014]. To the south and southeast of the Atlas mountain chain lies the West African Craton and Saharan platform [*Piqué et al*., 2002].

The Atlas mountains region has experienced widespread volcanism in the Cenozoic (Figure 2). The volcanism can be roughly divided into two phases [*Missenard and Cadoux*, 2012]: the first pulse of volcanism started in the beginning of the Cenozoic and the second, more voluminous phase, at about 11 Ma in the Miocene. These were separated by about a 20 Myrs gap in which no volcanic activity took place. The volcanism shows an alkaline intraplate chemical affinity [*Mokhtari and Velde*, 1988; *Rachdi et al*., 1997; *El Azzouzi et al*., 2010, 1999; *Wagner et al*., 2003], except for the three provinces in the North, closest to the Mediterranean Sea (Figure 2), which are calc-alkaline to alkaline and related also to the Rif subduction system [*Coulon et al*., 2002; *Maury et al*., 2000].

An anomalously thin lithosphere exists beneath the Atlas mountains as a semicontinuous zone from the Atlantic margin to the Africa-Eurasia plate boundary in the northeast, named the "Moroccan Hot Line" [*Frizon de Lamotte et al*., 2009] and situated beneath most of the Cenozoic volcanic provinces of the region. The width of this zone varies from 200 to 500 km and the lithosphere thickness is 60 to 90 km according to geopotential field studies [*Fullea et al*., 2010; *Missenard et al*., 2006]. Seismic studies also show thin lithosphere in this area with high Sn attenuation and low Pn velocities, some suggesting lithosphere-asthenosphere boundaries as shallow as 50 km [*Palomeras et al*., 2014; *Seber et al*., 1996; *Calvert et al*., 2000]. S/SKS splitting shows localized asthenospheric flow in the Middle Atlas and Central High Atlas parallel to the trend of the mountain chains [*Miller et al*., 2013]. The thinning has been attributed to delamination of the Atlas mountain root [*Duggen*, 2005; *Bezada et al*., 2014; *Ramdani*, 1998] and edge-driven convection [*Missenard and Cadoux*, 2012]. The observation that the Cenozoic volcanism of the region is similar in composition to the plume derived volcanism at the Canary Islands [*Duggen et al*., 2009] has led to the proposition that the thinned zone acts as a corridor for the hot plume material, causing the volcanism in the Atlas region.

2. Methods

To model the EDC we solve the nondimensional equations of conservation of mass, momentum, and energy using finite element mantle convection code Citcom [*Moresi and Gurnis*, 1996; *Zhong et al*., 2000].

Table 1. Model Input Parameters Used

Parameter	Symbol and Units	Value(s) Used
Water content	X_{H_2O}, ppm wt	100, 200, 300, 400
Activation energy	E, kJ mol^{-1},	120, 150, 180, 210, 240, 270
Radiogenic heating	Q, $10^{-12}\times$W kg^{-1}	12, 19, 27
Activation volume	V, m^3 mol^{-1}	6×10^{-6}
Reference temperature	$T_{abs,0}$, K	1623
Reference pressure	P_0, Pa	21.4×10^9 (660 km depth)
Reference viscosity	η_0, Pa s	10^{24}
Reference density	ρ_0, kg m^{-3}	3300
Thermal diffusivity	κ, m^2 s^{-1}	10^{-6}
Latent heat of melting	L, kJ kg^{-1}	560
Coefficient of thermal expansion	α, K^{-1}	3.5×10^{-5}

The effects of shear heating, adiabatic heating, and latent heat of melting are accounted for via the extended Boussinesq approximation [*Christensen and Yuen*, 1985]. The models consist of 3960 km (x 3960 km) x 660 km domain (x-z in 2-D and x-y-z in 3-D case) representing upper mantle and crust. An area of high lithosphere thickness is imposed with an artificially high (100 times larger) viscosity block on the left of the model domain, from $x=0$km to $x=990$km, extending to depth of $z=200$km, representing the more viscous cratonic lithosphere, the proton. The tecton with thin lithosphere has normal mantle viscosity. The initial thermal structure (thickness) of the lithosphere is the steady state thickness, attained after prolonged model run time prior to examination of EDC related processes (see also discussion in 4.2.). The steady state is defined to be reached when the average lithosphere thickness grows by less than 0.1% in one million years. This test for steady state is performed on each of the models separately so that each model with different parameters has its own initial temperature field consistent with the imposed parameters.

We have imposed closed free-slip stress boundary conditions at each boundary and zero heat flow at each boundary except for the surface for which $T=0°$C. To maintain a stable realistic mantle potential temperature without additional heating from the bottom boundary, we have increased the radiogenic heating values of the mantle (Table 1) to between 1.5 and 3.7 times higher than the modern-day mantle values (7.38×10^{-12} W kg^{-1}) [*Schubert et al*., 2001]. The advantage of using internal heating to maintain the model temperature instead of bottom heating is that the rate of thermal plume generation at the transition zone is greatly diminished. This helps in identifying the thermal anomalies at lithosphere-asthenosphere boundary caused by EDC alone. The higher values of radiogenic heating can also be used to reflect the style of EDC in the early Earth.

We have incorporated the hydrous peridotite melting parameterization of *Katz et al*. [2003] to study the amounts of melts produced by the EDC. The compositional fields (water content and depletion) are advected using a marker-in-cell method [e.g., *Gerya and Yuen*, 2003] with a second order Runge-Kutta scheme. The amount of melting in each marker is calculated each time step, and any melt produced is removed assuming instantaneous percolation to the surface. The amount of water removed with the melts is calculated assuming batch melting and water incompatibility with bulk partition coefficient of $D = 0.01$. After melting, the depletion value $F_{\%}=100F$ of each marker is adjusted. The depletion affects the buoyancy of the mantle using the following parameterization:

$$\frac{\mathrm{d}\ln\rho}{\mathrm{d}F_{\%}} = -0.00020 \tag{1}$$

from *Schutt and Lesher* [2006], which is applicable at pressures of about 3 GPa.

Linear, temperature and pressure dependent viscosity parameterization for olivine rheology [*Karato and Wu*, 1993] is applied:

$$\eta_{dry} = \eta_0 \exp\left(\frac{E+PV}{RT_{abs}}\right)\exp\left(-\frac{E+P_0V}{RT_{abs,0}}\right), \tag{2}$$

where E and V are the activation energy and volume, respectively, R is the gas constant, T_{abs} is the absolute temperature, and P the pressure (see Table 1 for values.) $T_{abs,0}$ and P_0 are the reference temperature and pressure in which conditions the viscosity has the reference value η_0. Because adiabatic heating has been used, there is no single location in the model domain where $T=T_0$ and $P=P_0$, and thus η_0 does not represent mantle viscosity directly at any particular location.

Reduced values for activation energy E have been used to "mimic" the behavior of nonlinear rheology at the shallow level of the mantle, the lithosphere-asthenosphere boundary. This circumvents the added

complexity of finding suitable rheology parameters for a long-term steady state model in a nonlinear viscosity case. The initial conditions for nonlinear rheology models of small-scale convection are even more critical than those of linear rheology models [*Sleep*, 2007]. As shown by *Christensen* [1984], multiplying the activation enthalpy ($H=E+PV$) value of the Newtonian rheology formulation by a factor of $\beta < 1$ produces similar steady state convection patterns than a nonlinear rheology with normal activation enthalpy. The exact value of β depends on the ratio of E and V. In a temperature dominated rheology (high E/V), such as ours, *Christensen* [1984] suggests that $\beta=0.3 \ldots 0.5$ would be a suitable value. Furthermore, *van Hunen et al*. [2005] have shown that lowering the activation energy from 360 to 120 kJ mol^{-1} in a Newtonian rheology increases the thermomechanical erosion of the lithosphere and causes thermal boundary layer instability similar to non-Newtonian ($n = 3.5$, $E=540$ kJ mol^{-1}) rheology. In our parameter study we have used low values for the activation energy but varied them to study the effect of rheology on EDC dynamics (Table 1).

To account for the viscosity lowering effect of water, we use a water weakening parameterization

$$\eta_{hydrous}=W\eta_{dry}, \quad W=100^{\frac{-X_{H_2O}}{X_{H_2O}+a}}, \tag{3}$$

as used by *Kaislaniemi et al*. [2014]. X_{H_2O} is the water content (wt ppm), and a (wt ppm) is a parameter controlling the sensitivity of water weakening (i.e., how large X_{H_2O} needs to be to decrease viscosity by one order of magnitude). This parameterization conforms to the boundary conditions set by experimental results [*Kohlstedt et al*., 1995; *Hirth and Kohlstedt*, 1996; *Mei and Kohlstedt*, 2000; *Bai and Kohlstedt*, 1992]: viscosity is inversely proportional to the water fugacity, and, at low water contents, water fugacity is proportional to the water content, i.e., $\eta \propto C_{OH}^{-r}$, where C_{OH} is the water (hydroxyl ion) concentration in olivine, and r is a constant close to one. Also, there should be a maximum limit for the weakening. *Karato* [2010] reports maximum viscosity weakening by water of four orders of magnitude, whereas *Fei et al*. [2013] reports maximum weakening by less than 1 order of magnitude. We use a commonly used value from *Hirth and Kohlstedt* [1996] who report maximum weakening of about two orders of magnitude. Our parameterization asymptotically approaches this value as water content increases. The water weakening parameterization used here has an additional advantage that it allows the water content to approach zero during melt removal, while still producing finite viscosity estimations values.

The lower end of the used water content values represent asthenospheric background concentrations, i.e., those present in mid-oceanic ridge basalt source mantle (∼120 wt ppm) *Dixon et al*. [2004]. High water content values are used to test the effect of mantle hydration on edge-driven convection in scenarios where the edge is situated near to a source of water, e.g., a recent subduction zone.

The amount of melting (volcanism) is calculated by assuming that all melt percolates instantly to the surface. The amount of uplift is estimated by calculating the corresponding layer thickness (with $\rho=2800$ kg m^3) needed to compensate the vertical stress at the upper boundary of the model.

Detailed methodology is available as supporting information.

3. Results

3.1. General Convection Patterns of the EDC

An edge-driven convection pattern forms at the transition from the thin tecton lithosphere to the thicker proton lithosphere (Figure 3). The style of the convection periodically changes from what looks like EDC s.s. (Figure 3a), but with a smaller convection cell size, to purely EDC w.s. style convection (Figure 3b) where the horizontal flow completely overrules the downwelling cold flow. This competition between horizontal flow and the cold downwelling produces periodic behavior in the flow. The horizontal flow is initially caused by the insulating effect of the thicker proton lithosphere, which keeps the mantle below the proton warmer than elsewhere. Once the horizontal flow is formed it causes a large-scale convection cell and a return flow to below the proton in the lower part of the upper mantle, which maintains the flow induced by continental insulation.

In the EDC convection cell the upwelling mantle material erodes the bottom of the lithosphere. Upwellings also make decompression melting possible. Where any melts are removed, a layer of depleted material (in black in Figure 3) is left behind. This drier (more viscous) and depleted (more buoyant) material tends to

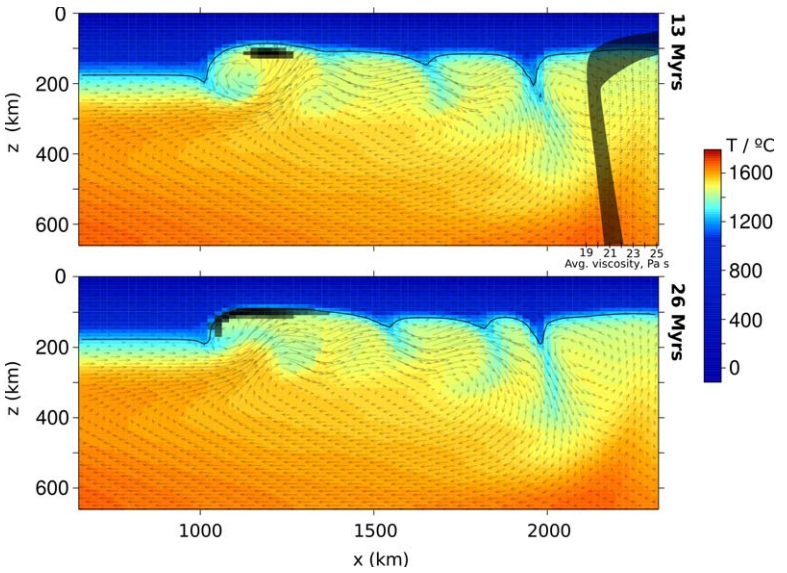

Figure 3. Two end-members of the EDC: downwelling dominated (above, similar to EDC s.s.) and upwelling dominated (below, EDC with shear), occurring in same model but separated by about 13 Myrs. Regions of melting depleted mantle in black. The shaded profile on the right in the upper figure shows the range of horizontal average viscosity values of the tecton domain in all of the 2-D models.

stick to the bottom of the lithosphere, from where it and pieces of lithosphere are later being partly delaminated by the erosional effect of the EDC convection cell (Figure 4).

3.2. Parameter Study Results

The chosen model input parameters (Table 1) result in models with a range of different mantle potential temperatures (1290−1472°C) and different average (statistically steady state) lithospheric thicknesses (1250°C isotherm at h_{te}=96−184km and h_{pr}=158−206km for tecton and proton lithospheres, respectively). The EDC convection pattern is present in all of the models. The horizontal potential temperature differences between the sublithospheric mantles of the tecton and the proton, $\Delta T_{pr/te}$, range between 8−61°C. The amount of lithospheric thinning, Δh_{ed} (see Figure 1a), which is the difference between the tecton lithosphere thickness (h_{te}) and the thickness (h_{ed}) at the thinnest part of lithosphere next to the proton-tecton edge, ranges between 11 and 51 km. The horizontal width of this thinned region is about 200 km.

Models show very clear pulsating nature in the EDC. This is evident as periodic uplift, lithospheric thinning/thickening, and magmatism at the edge (Figure 5), and from the convection patterns (Figure 3).

The periodicity of the melting varies between 14 and 26 Myrs among the models and is negatively correlated with the root mean square velocity of the model domain (Figure 6b). The periodicity of the lithosphere erosion has a larger variability among the models, but show similar trends to the melting periodicity, and often even equal periods as well. A correlation between the root mean square velocity and the model average mantle potential temperature and water contents can be found empirically (Figure 6d). Thus, the periods of uplift rate and melting (Figure 6b) negatively correlate with mantle potential temperature and water contents.

The amount of lithospheric thinning above the EDC convection cell is related to the activation energy of the viscosity parameterization (Figure 6a) and lithosphere thickness difference across the edge (Figure 6c). However, once melts are produced in the upper part of the EDC convection cell, the more viscous, slightly buoyant and colder depleted material gathers in the eroded lithosphere pocket (see Figure 3) and rethickens the lithosphere (i.e., reduces Δh_{ed}), as is evident from Figure 6a for models where magmatism >0 m Myr^{-1}.

The effect of lithosphere thickness difference across the edge on the amount of lithospheric thinning at the edge is clearest with relatively cold models (Figure 6c). Models with high potential temperature (and thus also with lowest viscosities) show little variation in the amount of thinning and the thinning in these models is generally minor. However, because of high temperatures, not so much thinning is required to allow the

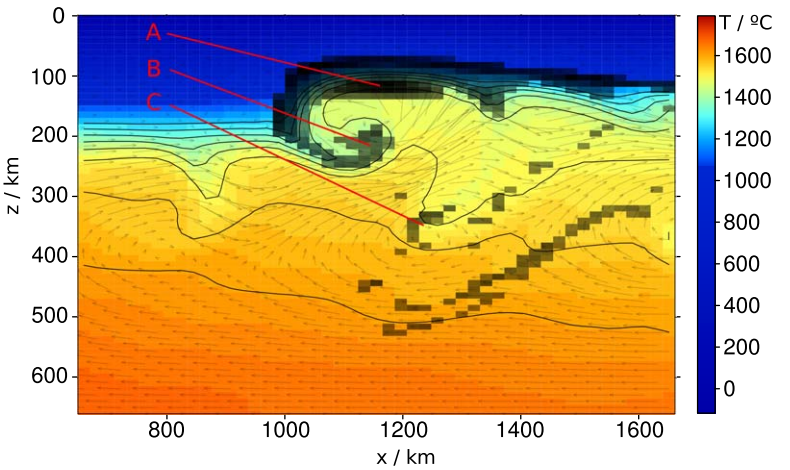

Figure 4. Temperature and depletion field in detail near the edge. Depleted material (in black) forms after decompression melting at the upper part of the EDC convection cell ("A"). It then sticks to the bottom of the lithosphere where it is being dragged horizontally by the asthenospheric flow. The shear caused by the EDC convection cell delaminates pieces of lithosphere together with depleted material ("B"). Relatively cold delaminated pieces with depleted material in them can sink deep into the mantle ("C") before being mechanically mixed with rest of the mantle by the background mantle flow. For comparison to tomography results, see section 4.1.

asthenospheric flow cross the solidus and melt. The three separate groups are formed by different internal heating values, and the negative trends within these groups are formed by the variation of the activation energy E (lowest values producing thinnest tecton thicknesses).

The amount of melt produced by EDC is mainly a function of the tecton lithosphere thickness. This tecton lithosphere thickness, on the other hand, depends on the effective average viscosity of the mantle, or, in other words, mantle potential temperature, mantle water contents, and mantle's rheological activation

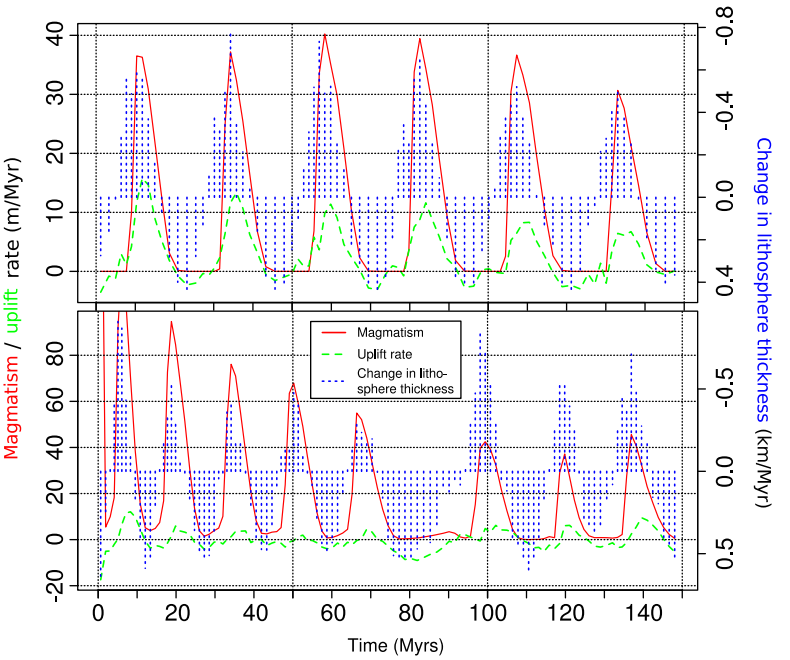

Figure 5. The history of uplift and magmatism in two of the models, discussed in relation to the Moroccan Atlas mountains (section 4.1). Values are measured at the location of maximum lithospheric thinning (Δh_{ed}) near the edge. Models not plotted here show varying amounts of correlation between these periods (see Figure 6b), but all show that the change in the lithosphere thickness systematically precedes the maximum of the magmatism. The models shown here are marked with circles in all plots in Figure 6. Models have following parameters: (a) $X_{H_2O}=200$ppm, $Q=19\times10^{-12}$Wkg^{-1}, $E=120$kJmol^{-1}, (b) same as Figure 5a but with $X_{H_2O}=400$ppm. Resulting temperatures are: (a) $T_{pot}=1388$°C, $\Delta T_{pot,pr/te}=41$°C, (b) $T_{pot}=1358$°C, $\Delta T_{pot,pr/te}=25$°C.

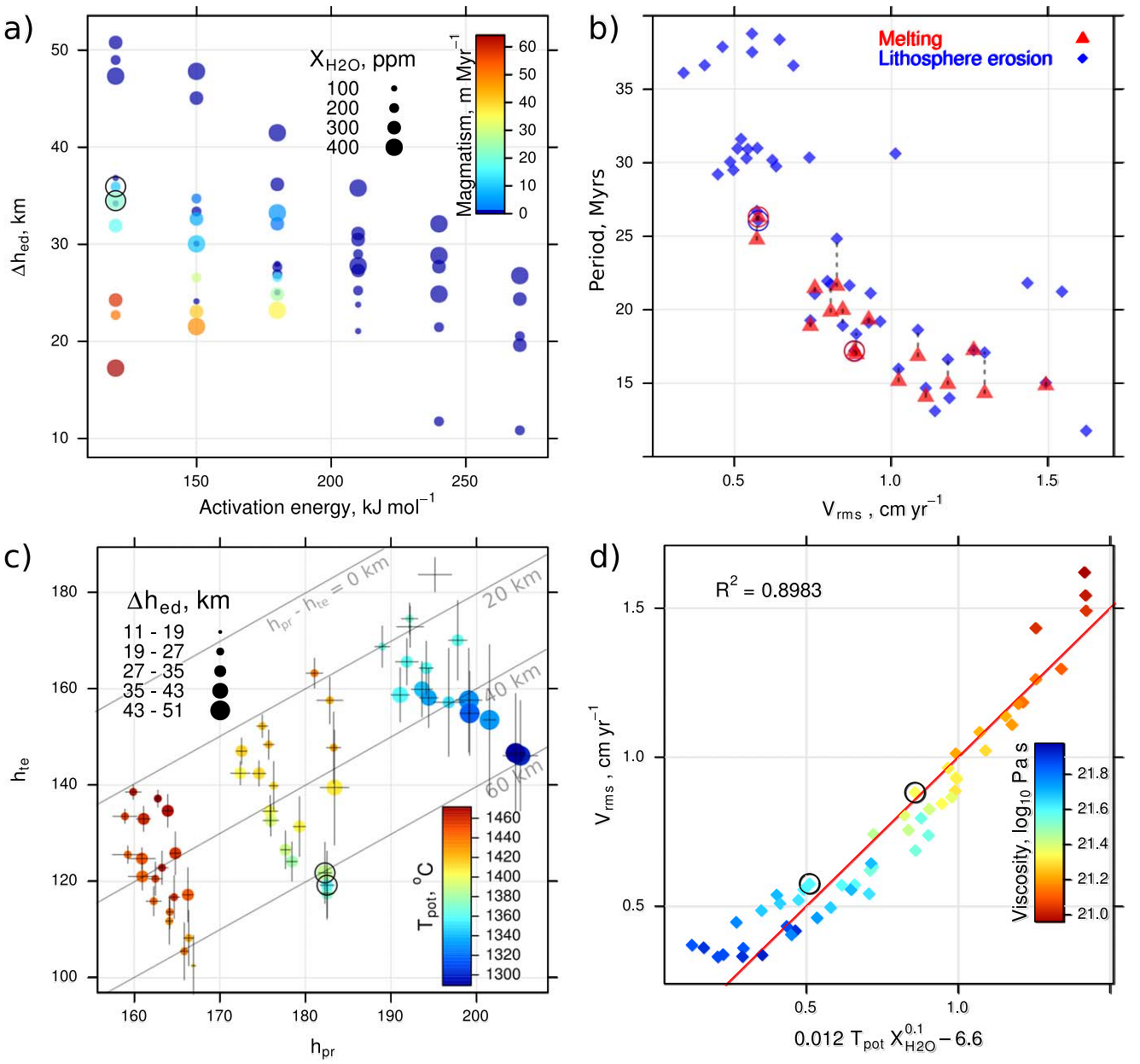

Figure 6. Parameter study results from the 2-D models. (a) The negative correlation between the activation energy value in the viscosity parameterization and the produced lithosphere thinning near the edge. Models where melts are produced start to deviate from the linear relationship as the melt residue at the top of the EDC convection cell decreases the thermal lithosphere thickness. Models with low water contents produce generally less thinning. (b) Relationship between the model root mean square velocity and the period of melting events or lithosphere thickness variation near the edge. Dashed lines connect models with same set of input parameters. Note that the melting period has been only plotted for models where melts are produced. There are eight models in which lithospheric erosion period is either nonexistent or too long to be determined within the 150 Myrs model run time. (c) Amount of lithosphere thinning near the edge as a function of proton and tecton lithosphere thicknesses and average mantle potential temperature. Error bars show the variation (standard deviation) in the lithosphere thicknesses. Isolines of lithosphere thickness difference (proton-tecton) has been plotted in the background. (d) Model data points and best empirical fit of model root mean square velocity as a function of mantle potential temperature and water content. The linear relationship is good and indicates that horizontal axis in Figure 6b could be expressed also in terms of potential temperature and water content. (a–d) Circled models are those shown in Figure 5 and discussed in Discussion in relation to the Moroccan Atlas mountains.

energy. A negative correlation is found between amount of lithosphere thinning by EDC (Δh_{ed}) and amount of melt produced (Figure 6a). This counter-intuitive relationship is caused by two factors: 1) models with thin average tecton lithosphere cannot produce much more thinning via EDC as the thinning is even more effectively balanced by conductive cooling of the lithosphere; 2) melting consumes heat, cooling down the mantle, and produces high viscosity, slightly lower temperature depleted layer in the thinned lithosphere pocket, increasing the apparent thickness of the lithosphere (cf. Figure 6a). Amounts of melt produced (if

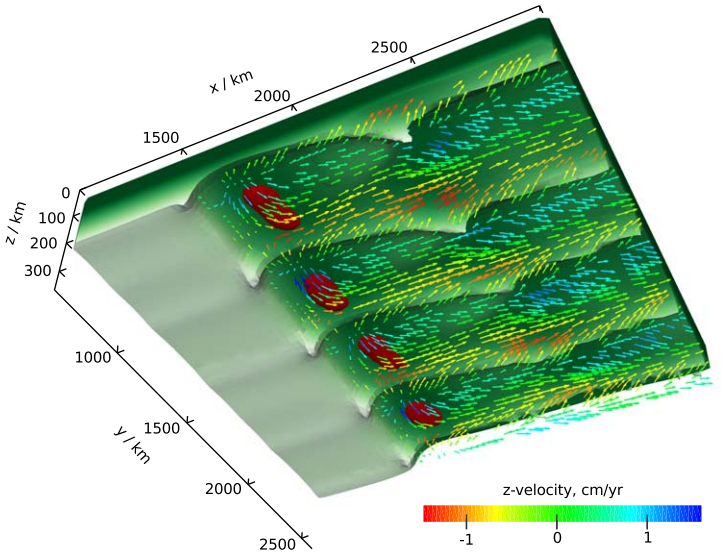

Figure 7. Three-dimensional structure of the EDC. The bottom of the lithosphere (1200°C isotherm) is shown in green. Dark red shows areas of active melting. Arrows show the velocity field at depth z=145 km, colors of the arrows indicating the velocity's z component. The edge-parallel flow (see text for discussion) can be seen near the melting pockets. Used model parameters are E=150 kJ mol^{-1}, Q=19×10^{-12} W kg^{-1}, X_{H_2O}=300 ppm.

produced at all) vary between zero and 60 m Myr^{-1} (average over 150 Myrs model time) for lithosphere average thinning amounts of about 40 to 20 km, respectively. If restricted to models with reasonable potential temperatures for today's Earth (1300–1400°C), amounts of melting and lithosphere thinning vary much less (5–20 m Myr^{-1}, 30 to 36 km, respectively).

3.3. Three-Dimensional Structure of EDC

Results from a 3-D model show the presence of the EDC but in addition indicates that the flow produced by the horizontal sublithospheric temperature difference produces convection rolls under the thinner tecton lithosphere with their axes perpendicular to the edge of the two lithospheric domains (Figure 7). In these rolls there is upflow on one side and downflow on the other side, while the overall flow is dominated by the horizontal sublithospheric flow. The horizontal flow is oriented away from the thicker proton lithosphere as in the 2D case, but there is also, especially near the edge, a significant horizontal velocity component parallel to the proton edge. This velocity component forms the upper part of the convection rolls or tubes that shape the lithosphere bottom. The existence of these rolls also affects the properties of the EDC along the edge. EDC is present in the middle of these rolls whereas in between the rolls the downwelling ridges effectively prohibits the formation of lithosphere erosion by EDC. This causes the melting regions of the EDC to be split into separate pockets along the edge.

4. Discussion

The style of the edge-driven convection shown in the results differs from the style envisaged by most previous studies on EDC. The cold downwelling at the edge of the lithosphere thickness gradient dominates the EDC *sensu stricto*, whereas in the results shown here the flow is governed by cold downwellings and hot upwellings in turns, resulting in the periodic nature of the EDC where EDC s.s. and EDC with shear alternate. For EDC w.s. to take place, higher sublithospheric mantle temperatures are needed beneath the thicker (proton) lithosphere. The horizontal temperature difference is modest, from 0.5 to 4% of the mantle potential temperature. This is in range of values found to be produced by continental insulation [*Heron and Lowman*, 2014]. Although it is unclear whether this amount of excess heat can account for supercontinent dispersion, our results show that even modest effect of insulation may change the mantle dynamics at the edge of the thick lithosphere. In our models the thicker lithosphere covers 25 % of the surface area, or, assuming symmetricity over z axis, represents a craton of 2000 km in width. This surface coverage is at

lower end of the scale used by *Heron and Lowman* [2014]. Larger coverage, with higher horizontal temperature difference, might have a strengthening effect on the EDC w.s.

We found a negative correlation between V_{rms} and $\Delta T_{pot,pr/te}$, which, although weaker than that found by *Heron and Lowman* [2014], is consistent with their observation that "the influence of continental insulation is seen to decrease as the vigor of convection is increased." The weakness of the correlation in our results is probably due to the other factors being varied in the input parameters (changes in viscous activation energy and water contents affecting effective viscosity).

A flow field similar to EDC w.s. could be produced by combination of purely downwelling driven EDC (EDC s.s.) combined with lithospheric plate movement relative to the underlying mantle (i.e., lithosphere moving to the left in Figure 1b) [cf. *Conrad et al*., 2010]. In this case no horizontal temperature difference (continental insulation) would be needed. However, in case of the Moroccan Atlas mountains (see below), this scenario is unlikely as the African plate has been moving (in fixed hotspot reference frame) more or less parallel to the craton edge [*Morgan and Morgan*, 2007].

Some of the models result in mantle potential temperatures that exceed values generally accepted for today's Earth. These results can be used to reflect the EDC process to earlier times in Earth's history or in a vicinity of a thermal anomaly in the modern Earth's mantle. Consistent with the negative correlation between V_{rms} and $\Delta T_{pot,pr/te}$, the models with higher temperatures (and thus, generally higher V_{rms}) show smaller amounts of lithospheric erosion due to EDC (Figure 6c). Largest amount of lithospheric thinning is produced in the colder models, although these often show exceptionally high (tecton) lithospheric thicknesses. For EDC to be most effective in lithospheric thinning, a low value of viscous activation energy is needed ("mimicking" nonlinear rheology, see Methods). Using low values of activation energy thickens the rheological transition layer between asthenosphere and lithosphere, making the lithosphere-asthenosphere viscosity change more gradual and thus allowing easier erosion into this boundary layer (see discussion in 4.2. below).

No model with the smallest amount of water (100 ppm) produced melting (see Figure 6a), but models with 200 ppm or more water produce significant amounts of melting, suggesting that there is a rather abrupt change from no-melting domain to melt producing domain. This is due to the effect of water which lowers the mantle solidus but also enhances the lithosphere thinning near the edge via the exponential effect on mantle viscosity. A threshold for melting caused by the mantle water contents could also explain why volcanism by edge-driven convection is not a global phenomenon: mantle regions close to recent subduction zones might be slightly more hydrated than those far away, e.g., passive margins.

4.1. Application to Moroccan Atlas Mountains and the 3-D Structure

The results support the hypothesis that the Cenozoic magmatism and related uplift in the Moroccan Atlas mountains has been produced by edge-driven convection [*Missenard and Cadoux*, 2012]. It seems plausible that the style of EDC operating at the West African craton boundary is a combination of EDC *sensu stricto* and EDC with shear. These conclusions are supported by the following observations:

1) Estimated lithospheric thicknesses at the Atlas mountains area are: northwestern domain (Moroccan Meseta) 100–120 km, the craton side of the Atlas mountains about 180 km, and the lithosphere underneath the Atlas mountains about 80 km [*Teixell et al*., 2005]. This combination of lithospheric thicknesses (proton ~180 km, tecton ~110–120 km) and erosion (30–40 km) can be found among the models. (These two models are circled in all panels in Figure 6 and used to plot Figure 5. Parameters for these models can be found in the caption of Figure 5). This thinned part of the lithosphere in the middle varies in width between 300 and 400 km, compatible with results shown here (cf. Figure 3a). It is noteworthy that no tecton lithospheric thicknesses were imposed in any of the models, and that they and the amount of lithospheric thinning are purely functions of imposed parameters X_{H_2O}, Q and E.

2) The eruption rates in the volcanic provinces of the Atlas mountains vary between 1 and 30 m Myr^{-1} (total volume over covered area and duration of volcanism) during the volcanic phases [*Missenard and Cadoux*, 2012]. Results here show magmatic production rates up to 60 m Myr^{-1} averaged over the total model time (including nonvolcanic periods). The two models with compatible lithosphere thicknesses (point one above) show magmatic production rates of about 35 and 40–60 m Myr^{-1} during the volcanic phases. Even if not all

of the mantle magmatism erupt at the surface, the volumes produced are compatible with those observed in the field.

3) The periodicity of the mantle magmatism varies between 14 and 26 Myrs. For the two example models discussed the periods are 26 and 17 Myrs. These periods match well with the duration of the ~20 Myrs quiet gap between the volcanic episodes in the Atlas mountains [*Missenard and Cadoux*, 2012]. *Missenard and Cadoux* [2012] suggest this quiet gap is caused by the changes in the velocity of the African plate, but our results show that such episodicity is an inherent feature in the EDC w.s. and can be explained without external forcing from plate movements. Observations from duration of only one such volcanic period does not provide enough data to determine with certainty mechanisms responsible for it.

4) The three-dimensional structure of the EDC (Figure 7) shows that along the edge lithospheric erosion is not a continuous feature, but that the eroded "melting pockets" are separated by ridges of thicker lithosphere. This structure corresponds well to the tomographic results from the Atlas area [*Bezada et al*., 2014] (see Figure 2) that shows distinct areas of thinning along the Atlas mountains axis (the Western High Atlas, the Central High Atlas and the Middle Atlas). Distinct areas of thinning under Central High Atlas and Middle Atlas are also observable from the geophysical models of *Fullea et al*. [2010] (based on elevation, gravity, surface heat flow, and geoid height data). The nonexistence of single continuous thinned area under the Atlas mountains casts doubt on the hypothesis of a lithospheric corridor where the material of the Canarian mantle plume would flow northeast, as proposed by *Duggen et al*. [2009] on the basis of similar geochemistry of the volcanic rocks in the Atlas mountains region and the Canary island. However, the existence of a nearby plume could contribute to the decompression melting in the EDC by bringing in more fertile mantle material and more heat.

5) Based on their tomography results, *Bezada et al*. [2014] have suggested that the lithosphere underneath the Atlas mountains has experienced piecewise delamination. A fast Vp anomaly is located at 400 km depth in between the High and Middle Atlas, thought to represent a piece of delaminated lithosphere. Our models show that pieces of cold lithosphere with depleted asthenosphere incorporated in it can indeed be delaminated and brought into relatively deep mantle levels of 300–400 km (see Figure 4). The episodicity of the EDC w.s. can explain how the delamination under the Atlas mountains can take place piecewise. While our models utilize linear rheology parameterization, it is possible that a nonlinear rheology can produce avalanche-like behavior, where the erosion and delamination of the lithosphere is more punctuated than in linear rheology models [*van Hunen et al*., 2005].

The existence of partial melts in the melting pockets near the edge might also explain why the tomographic and gravity studies on lithosphere thickness in Atlas area generally agree but show small discrepancies in the absolute values of the lithosphere thickness [*Palomeras et al*., 2014]: The partial melts (and depleted asthenospheric material) might have effects of different scale on seismic velocities and on gravity field, having especially strong effect on seismic S velocities. Observations of seismic S/SKS velocity splitting [*Miller et al*., 2013], aligned parallel to the lithospheric edge and the Atlas mountains, can be understood if regarded as manifestation of the horizontal flow present in the upper part of the convection rolls shown in the three-dimensional EDC model (Figure 7).

The tearing of the Betic-Alboran slab along the northern edge of the African plate from the Middle Miocene onward [*Thurner et al*., 2014; *Spakman and Wortel*, 2004] may have contributed to the second, stronger pulse of the volcanism in the Atlas mountains. By allowing flow of hydrous mantle material from the overriding plate side of the subduction to the Atlas mountains area it could have enhanced the edge-driven convection, lithosphere erosion and melting.

4.2. Relations to Steady State Stagnant-Lid Convection Scaling Laws

Paying attention to the initial conditions of edge-driven convection models has been shown to be important [*Sleep*, 2007]. Models with laterally homogeneous lithosphere thicknesses can cause instabilities of similar magnitude as those caused by thickness variation in the lithosphere if unrealistic initial conditions are applied. Initial conditions have to provide a mature stagnant-lid convection regime before edge-driven convection processes are examined, so that the thickness of the thermal boundary layer below the lithosphere is in a statistical steady state condition. An unrealistically thick thermal boundary layer drives excess sublithospheric small-scale convection (effectively a collapse of this overthickened lithosphere), which could be mistaken for an instability caused by the edge in the lithosphere.

Because the effective viscosity (water content) and the activation energy in our viscosity parameterization (controlling the thermal boundary layer thickness) are varied, we ensure that the rheology used in the models with different parameters produces steady state stagnant lid convection. Test models with the same rheology as in the edge-driven convection models but with no imposed high-viscosity block (i.e., a laterally homogeneous lithosphere) has been run and resulting steady state heat flow compared to expected heat flow for stagnant-lid convection. The steady state heat flow to the bottom of the continental lithosphere and, in the absence of radiogenic heating, at the surface of the lithosphere has been suggested to scale as

$$q_{ss} = C_q k T_\eta^{4/3} \left[\frac{\rho g \alpha}{\kappa \eta_H}\right]^{1/3}, \tag{4}$$

where C_q is a constant with value ≈ 0.47, k is heat conductivity, T_η is a material property telling the temperature decrease needed to increase the viscosity by a factor of e, and η_H is the viscosity of the adiabatic half-space [*Sleep*, 2011; *Davaille and Jaupart*, 1993a, 1993b]. This scaling is for bottom-heated convection. Our models are internally heated, so we modify the equation to account for the heat flow component generated within the conductive lithosphere:

$$q_{ss,h} = C_q k T_\eta^{4/3} \left[\frac{\rho g \alpha}{\kappa \eta_H}\right]^{1/3} + Q \rho h_L, \tag{5}$$

where h_L is the thickness of the stagnant lid, defined as the upper part of the model where average velocities are less than 0.01% of the maximum velocity within the whole model.

Our test models produce a good fit with the steady state stagnant lid heat flow (black line in Figure 8) although with different value of constant C_q and an intercept point of vertical axis different from zero. These discrepancies are largely explained by the effect of radiogenic heating within the lithosphere: if radiogenic heating within the lithosphere is reduced from the measured surface heat flow values, i.e., equation (5) is applied, a slope much closer to $C_q = 0.47$ is found and the intercept with vertical axis is close to zero (red in Figure 8). The (thinner) tecton side of the actual edge-driven convection models are thus in a steady state stagnant lid convection regime at their initial stages and any additional instabilities are produced by the imposed edge in the lithosphere. Additionally, it can be concluded, that internally heated models of stagnant-lid convection adhere to the same scaling law as bottom-heated models.

Melting during the model run changes the amount of water, and thus viscosity, and buoyancy of the mantle via equations (1) and (3). This changes the values of ρ and T_η and/or η_H in equations (4) and (5). As the degree of melting and total depletion in the models turns out to be small and buoyancy is only linearly dependent on the depletion, the effect on buoyancy/density is small. However, the effect of depletion on viscosity is large, because the viscosity is inversely dependent on water content, which in turn has an exponential dependence on depletion. Viscosity increase caused by depletion is typically a factor of 2 to 5 in the models (locally). If depleted material remains in the convecting asthenosphere, η_H is affected, but the viscosity difference is quickly diluted via mechanical mixing, and the exponent $\frac{1}{3}$ in equation (4) makes the change in η_H to contribute to q_{ss} only in minor amounts. If, however, depleted material stays part of the lithosphere at its bottom, the effective value of T_η at the depleted region is decreased, as compositional viscosity increase replaces some of the temperature change needed to increase the viscosity. From scaling relationships given by *Sleep* [2007], the value of T_η can be related to the thickness ΔZ_{rheo} of the thermal boundary layer that participates in the sublithospheric small-scale convection:

$$\Delta Z_{\text{rheo}} \propto T_\eta^{-\frac{1}{3}}. \tag{6}$$

This relationship becomes almost linear in the range of interest ($50 < T_\eta < 150$K). As the erosion and accretion of the thermal boundary layer produces most of the lithosphere thickness variation measured in the models, we can locally, next to the lithosphere edge, relate $\Delta Z_{\text{rheo}} \propto \Delta h_{\text{ed}}$, with negative proportionality constant. Thus

$$\Delta h_{\text{ed}} \propto T_\eta^{-\frac{1}{3}}, \tag{7}$$

also with negative proportionality constant. The periodicity seen in the models (Figure 5) can now be understood as a repetition of following events: (1) Large ΔZ_{rheo} causes enhanced small-scale convection; (2)

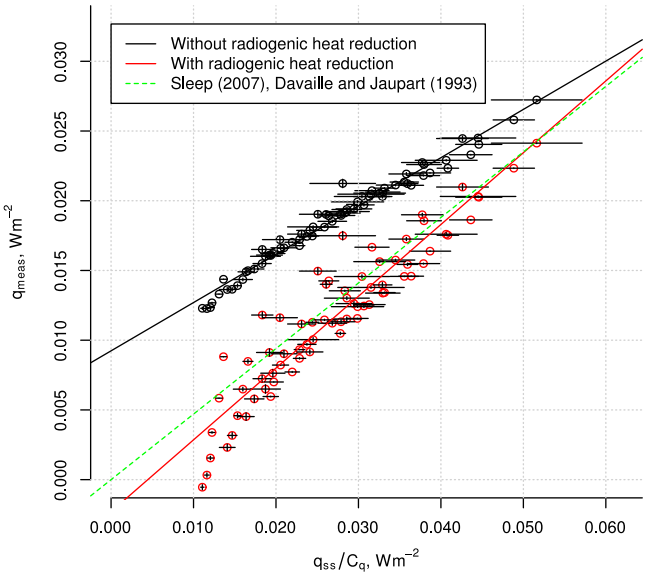

Figure 8. Stagnant lid heat flow, from scaling relationship versus measured surface values from the test models with no imposed lithosphere thickness variation. Circles represent time averaged values from models with different run parameters. Solid lines are best fit lines. Error bars show one standard deviation in time averaging. In red is shown the values from which the radiogenic heat production of the lithosphere (second term on the right in equation (5)) has been reduced. Green dashed line shows the slope $C_q = 0.47$, previously determined for bottom heated stagnant lid convection.

small-scale convection erodes the thermal boundary layer (ΔZ_{rheo} locally decreases, Δh_{ed} increases); (3) erosion allows decompression melting and gathering of depleted material; (4) more viscous depleted layer suppresses convective heating, allows conductive cooling, and thus an increase in ΔZ_{rheo}, decrease in T_η, and decrease in Δh_{ed} (7). This leads to 5) a situation similar to step 1, where the thermal boundary layer has thickened under the depleted layer. The depleted layer will be partially removed during subsequent lithosphere erosion (step 2 above). Similar chain of events can be recognized in sublithospheric small-scale convection [e.g., *Kaislaniemi et al.*, 2014] where no lithospheric edge is present. However, the edge in the lithosphere localizes the instabilities and allows more pronounced lithospheric erosion.

The effect of varying the activation energy on the amount of lithosphere thinning Δh_{ed} (Figure 6a), can be understood by examining the effect of E on T_η. The definition of T_η, that decreasing temperature from T_2 to T_1 increases viscosity by a factor of e, gives

$$\frac{\eta_0 \exp \frac{E+PV}{RT_1}}{\eta_0 \exp \frac{E+PV}{RT_2}} = e, \tag{8}$$

where

$$T_\eta = T_2 - T_1. \tag{9}$$

This leads to

$$T_\eta = T_2 - \left(\frac{R}{E+PV} + T_2^{-1} \right)^{-1}. \tag{10}$$

Increasing E thus produces decreasing T_η and, by (7), (almost linearly) decreasing Δh_{ed}, as in Figure 6a, where doubling E leads to reduction of Δh_{ed} by factor of $\sim\frac{1}{3}$, as shown by (7). Empirically, an inverse proportionality between E and T_η can be found in the range of interest (120kJ $\leq E \leq$ 270kJ).

5. Conclusions

Numerical models support the hypothesis that the primary reason for the Cenozoic volcanism and its spatial and temporal distribution in the Atlas mountains region is the sublithospheric edge-driven convection with a shearing component induced by continental insulation. These two different styles of edge-driven convection, alternating in a periodic manner, can explain the volcanism with ~20 Myrs quiet gap in the middle and the piecewise delamination of the lithosphere under the Atlas mountains. The three-dimensional lithospheric structure of the Atlas mountains region can be produced by edge-driven convection, causing non-continuous zone of thinned lithosphere parallel to the mountain chain, with pockets of lithosphere erosion and associated mantle melting.

Acknowledgments
The authors would like to thank an anonymous reviewer and Norman Sleep, whose comments and suggestions greatly improved the manuscript. Cin-Ty Lee is thanked for the editorial handling of the manuscript. The work has been funded by the European Union FP7 Marie Curie Initial Training Network Topomod, contract 264517 (Kaislaniemi); van Hunen acknowledges funding from the European Research Council (ERC Starting grant 279828).
This work made use of the facilities of N8 HPC provided and funded by the N8 consortium and EPSRC (Grant No. EP/K000225/1). The Centre is co-ordinated by the Universities of Leeds and Manchester.

References

Bai, Q., and D. L. Kohlstedt (1992), Substantial hydrogen solubility in olivine and implications for water storage in the mantle, *Nature*, *357*, 672–674.

Beauchamp, W., R. W. Allmendinger, M. Barazangi, A. Demnati, M. El Alji, and M. Dahmani (1999), Inversion tectonics and the evolution of the High Atlas Mountains, morocco, based on a geological-geophysical transect, *Tectonics*, *18*(2), 163–184.

Bezada, M. J., E. D. Humphreys, J. Davila, R. Carbonell, M. Harnafi, I. Palomeras, and A. Levander (2014), Piecewise delamination of Moroccan lithosphere from beneath the Atlas Mountains, *Geochem. Geophys. Geosyst.*, doi:10.1002/2013GC005059, in press.

Calvert, A., E. Sandvol, D. Seber, M. Barazangi, S. Roecker, T. Mourabit, F. Vidal, G. Alguacil, and N. Jabour (2000), Geodynamic evolution of the lithosphere and upper mantle beneath the Alboran region of the western Mediterranean: Constraints from travel time tomography, *J. Geophys. Res.*, *105*(B5), 10,871–10,898.

Christensen, U. (1984), Convection with pressure- and temperature-dependent non-Newtonian rheology, *Geophys. J. R. Astron. Soc.*, *77*, 343–384.

Christensen, U. R., and D. A. Yuen (1985), Layered convection induced by phase transitions, *J. Geophys. Res.*, *90*(B12), 10,291–10,300.

Conrad, C. P., B. Wu, E. I. Smith, T. A. Bianco, and A. Tibbetts (2010), Shear-driven upwelling induced by lateral viscosity variations and asthenospheric shear: A mechanism for intraplate volcanism, *Phys. Earth Planet. Inter.*, *178*(3-4), 162–175, doi:10.1016/j.pepi.2009.10.001.

Coulon, C., M. Megartsi, S. Fourcade, R. C. Maury, H. Bellon, A. Louni-hacini, J. Cotten, A. Coutelle, and D. Hermitte (2002), Post-collisional transition from calc-alkaline to alkaline volcanism during the Neogene in Oranie (Algeria): Magmatic expression of a slab breakoff, *Lithos*, *62*, 87–110.

Davaille, A., and C. Jaupart (1993a), Thermal convection in lava lakes, *Geophys. Res. Lett.*, *20*(17), 1827–1830.

Davaille, A., and C. Jaupart (1993b), Transient high-Rayleigh-number thermal convection with large viscosity variations, *J. Fluid Mech.*, *253*, 141–166, doi:10.1017/S0022112093001740.

Dixon, J. E., T. H. Dixon, D. R. Bell, and R. Malservisi (2004), Lateral variation in upper mantle viscosity: Role of water, *Earth Planet. Sci. Lett.*, *222*(2), 451–467, doi:10.1016/j.epsl.2004.03.022.

Duggen, S. (2005), Post-Collisional Transition from subduction- to intraplate-type magmatism in the Westernmost Mediterranean: Evidence for continental-edge delamination of subcontinental lithosphere, *J. Petrol.*, *46*(6), 1155–1201, doi:10.1093/petrology/egi013.

Duggen, S., K. A. Hoernle, F. Hauff, A. Klugel, M. Bouabdellah, and M. Thirlwall (2009), Flow of Canary mantle plume material through a subcontinental lithospheric corridor beneath Africa to the Mediterranean, *Geology*, *37*(3), 283–286, doi:10.1130/G25426A.1.

El Azzouzi, M., J. Bernard-Griffiths, H. Bellon, R. C. Maury, A. Piqué, S. Fourcade, J. Cotten, and J. Hernandez (1999), Évolution des sources du volcanisme marocain au cours du Néogène, *C. R. Acad. Sci. Ser. II*, *329*, 95–102.

El Azzouzi, M., R. C. Maury, H. Bellon, N. Youbi, J. Cotten, and F. Kharbouch (2010), Petrology and K-Ar chronology of the Neogene-Quaternary Middle Atlas basaltic province, Morocco, *Bull. Soc. Geol. Fr.*, *181*(3), 243–257.

Elder, J. (1976), *The Bowels of the Earth*, 222 pp., Oxford Univ. Press, Oxford, U. K.

Farr, T. G., et al. (2007), The Shuttle Radar Topography Mission, *Rev. Geophys.*, *45*, RG2004, doi:10.1029/2005RG000183.

Fei, H., M. Wiedenbeck, D. Yamazaki, and T. Katsura (2013), Small effect of water on upper-mantle rheology based on silicon self-diffusion coefficients, *Nature*, *498*(13 June), 213–215, doi:10.1038/nature12193.

Frizon de Lamotte, D., B. S. Bezar, and R. Bracène (2000), The two main steps of the Atlas building and geodynamics of the western Mediterranean, *Tectonics*, *19*(4), 740–761.

Frizon de Lamotte, D., P. Leturmy, Y. Missenard, S. Khomsi, G. Ruiz, O. Saddiqi, F. Guillocheau, and A. Michard (2009), Mesozoic and Cenozoic vertical movements in the Atlas system (Algeria, Morocco, Tunisia): An overview, *Tectonophysics*, *475*(1), 9–28, doi:10.1016/j.tecto.2008.10.024.

Fullea, J., M. Fernàndez, J. Afonso, J. Vergés, and H. Zeyen (2010), The structure and evolution of the lithosphere-asthenosphere boundary beneath the Atlantic-Mediterranean Transition Region, *Lithos*, *120*(1-2), 74–95, doi:10.1016/j.lithos.2010.03.003.

Gerya, T. V., and D. A. Yuen (2003), Characteristics-based marker-in-cell method with conservative finite-differences schemes for modeling geological flows with strongly variable transport properties, *Phys. Earth Planet. Inter.*, *140*(4), 293–318, doi:10.1016/j.pepi.2003.09.006.

Gomez, F., R. Allmendinger, M. Barazangi, A. Er-Raji, and M. Dahmani (1998), Crustal shortening and vertical strain partitioning in the Middle Atlas Mountains of Morocco, *Tectonics*, *17*(4), 520–533.

Griffin, W., S. O'Reilly, N. Abe, S. Aulbach, R. Davies, N. Pearson, B. Doyle, and K. Kivi (2003), The origin and evolution of Archean lithospheric mantle, *Precambrian Res.*, *127*, 19–41, doi:10.1016/S0301–9268(03)00180-3.

Gurnis, M. (1988), Large-scale mantle convection and the aggregation and dispersal of supercontinents, *Nature*, *332*, 695–699.

Hardebol, N. J., R. N. Pysklywec, and R. Stephenson (2012), Small-scale convection at a continental back-arc to craton transition: Application to the southern Canadian Cordillera, *J. Geophys. Res.*, *117*, B01408, doi:10.1029/2011JB008431.

Heron, P. J., and J. P. Lowman (2014), The impact of Rayleigh number on assessing the significance of supercontinent insulation, *J. Geophys. Res. Solid Earth*, *119*, 711–733, doi:10.1002/2013JB010484.

Hirth, G., and D. L. Kohlstedt (1996), Water in the oceanic upper mantle: Implications for rheology, melt extraction and the evolution of the lithosphere, *Earth Planet. Sci. Lett.*, *144*, 93–108.

Janse, A. (1994), Is Clifford's rule still valid? Affirmative examples from around the world, in *Diamonds: Characterization, Genesis and Exploration*, edited by H. Meyer and O. Leonardos, pp. 215–235, Dep. Nac. da Prod. Mineral., Brazil.

Kaislaniemi, L., J. van Hunen, M. B. Allen, and I. Neill (2014), Sublithospheric small-scale convection—A mechanism for collision zone magmatism, *Geology*, *42*(4), 291–294, doi:10.1130/G35193.1.

Karato, S.-i. (2010), Rheology of the deep upper mantle and its implications for the preservation of the continental roots: A review, *Tectonophysics*, *481*(1-4), 82–98, doi:10.1016/j.tecto.2009.04.011.

Karato, S.-i., and P. Wu (1993), Rheology of the upper mantle: A synthesis, *Science*, *260*(5109), 771–778.

Katz, R. F., M. Spiegelman, and C. H. Langmuir (2003), A new parameterization of hydrous mantle melting, *Geochem. Geophys. Geosyst.*, *4*(9), 1073, doi:10.1029/2002GC000433.

King, S. D. (2000), African Hot Spot Volcanism: Small-Scale Convection in the Upper Mantle Beneath Cratons, *Science*, *290*(5494), 1137–1140, doi:10.1126/science.290.5494.1137.

King, S. D. and D. L. Anderson (1995), An alternative mechanism of flood basalt formation, *Earth Planet. Sci. Lett.*, *136*(3-4), 269–279.

King, S. D. and D. L. Anderson (1998), Edge-driven convection, *Earth Planet. Sci. Lett.*, *160*(3-4), 289–296.

Kohlstedt, D. L., B. Evans, and S. J. Mackwell (1995), Strength of the lithosphere: Constraints imposed by laboratory experiments, *J. Geophys. Res.*, *100*(B9), 17,587–17,602.

Maury, R. C., et al. (2000), Post-collisional Neogene magmatism of the Mediterranean Maghreb margin: A consequence of slab breakoff, *C. R. Acad. Sci. Ser. II*, *331*(3), 159–173, doi:10.1016/S1251-8050(00)01406-3.

Mei, S., and D. Kohlstedt (2000), Influence of water on plastic deformation of olivine aggregates 1. Diffusion creep regime, *J. Geophys. Res.*, *105*(B9), 21,457–21,469.

Miller, M. S., and T. W. Becker (2014), Reactivated lithospheric-scale discontinuities localize dynamic uplift of the Moroccan Atlas Mountains, *Geology*, *42*(1), 35–38, doi:10.1130/G34959.1.

Miller, M. S., A. A. Allam, T. W. Becker, J. F. Di Leo, and J. Wookey (2013), Constraints on the tectonic evolution of the westernmost Mediterranean and northwestern Africa from shear wave splitting analysis, *Earth Planet. Sci. Lett.*, *375*, 234–243, doi:10.1016/j.epsl.2013.05.036.

Missenard, Y., and A. Cadoux (2012), Can Moroccan Atlas lithospheric thinning and volcanism be induced by Edge-Driven Convection?, *Terra Nova*, *24*(1), 27–33, doi:10.1111/j.1365-3121.2011.01033.x.

Missenard, Y., H. Zeyen, D. Frizon de Lamotte, P. Leturmy, C. Petit, M. Sébrier, and O. Saddiqi (2006), Crustal versus asthenospheric origin of relief of the Atlas Mountains of Morocco, *J. Geophys. Res.*, *111*, B03401, doi:10.1029/2005JB003708.

Mokhtari, A., and D. Velde (1988), Xenocrysts in Eocene camptonites from Taourirt, northern Morocco, *Mineral. Mag.*, *52*, 587–601.

Moresi, L., and M. Gurnis (1996), Constraints on the lateral strength of slabs from three-dimensional dynamic flow models, *Earth Planet. Sci. Lett.*, *138*, 15–28.

Morgan, W. J., and J. P. Morgan (2007), Geological Society of America Special Papers, *Geol. Soc. Am. Spec. Pap.*, *430*, 65–78, doi:10.1130/2007.2430(04).

Palomeras, I., S. Thurner, a. Levander, K. Liu, a. Villasenor, R. Carbonell, and M. Harnafi (2014), Finite-frequency Rayleigh wave tomography of the western Mediterranean: Mapping its lithospheric structure, *Geochem. Geophys. Geosyst.*, *15*, 140–160, doi:10.1002/2013GC004861.

Piqué, A., P. Tricart, R. Guiraud, E. Laville, S. Bouaziz, M. Amrhar, and R. A. Ouali (2002), The Mesozoic-Cenozoic Atlas belt (North Africa): An overview, *Geodin. Acta*, *15*(3), 185–208, doi:10.1080/09853111.2002.10510752.

Rachdi, H., M. Berrahma, M. DeLaloye, A. Faure-Muret, and M. Dahmani (1997), Le volcanisme tertiaire du Rekkame (Maroc): Pétrologie, géochimie et géochronologie, *J. Afr. Earth Sci.*, *24*(3), 259–269.

Ramdani, F. (1998), Geodynamic implications of intermediate-depth earthquakes and volcanism in the intraplate Atlas mountains (Morocco), *Phys. Earth Planet. Inter.*, *108*, 245–260.

Schubert, G., D. L. Turcotte, and P. Olson (2001), *Mantle Convection in the Earth and Planets*, 940 pp., Cambridge Univ. Press, Cambridge, U. K.

Schutt, D. L., and C. E. Lesher (2006), Effects of melt depletion on the density and seismic velocity of garnet and spinel lherzolite, *J. Geophys. Res.*, *111*, B05401, doi:10.1029/2003JB002950.

Seber, D., M. Barazangi, B. A. Tadili, M. Ramdani, A. Ibenbrahim, and D. B. Sari (1996), Three-dimensional upper mantle structure beneath the intraplate Atlas and interplate Rif mountains of Morocco, *J. Geophys. Res.*, *101*(B2), 3125–3138.

Shahnas, M. H., and N. P. Russell (2004), Anomalous topography in the western Atlantic caused by edge-driven convection, *Geophys. Res. Lett.*, *31*, L18611, doi:10.1029/2004GL020882.

Sleep, N. H. (2007), Edge-modulated stagnant-lid convection and volcanic passive margins, *Geochem. Geophys. Geosyst.*, *8*, Q12004, doi:10.1029/2007GC001672.

Sleep, N. H. (2011), Small-scale convection beneath oceans and continents, *Chin. Sci. Bull.*, *56*(13), 1292–1317, doi:10.1007/s11434-011-4435-x.

Spakman, W., and M. J. R. Wortel (2004), Tomographic View on Western Mediterranean Geodynamics, in *The TRANSMED Atlas. The Mediterranean Region from Crust to Mantle*, edited by W. Cavazza et al., pp. 31–52, Springer, Berlin.

Teixell, A., M.-L. Arboleya, M. Julivert, and M. Charroud (2003), Tectonic shortening and topography in the central High Atlas (Morocco), *Tectonics*, *22*(5), 1051, doi:10.1029/2002TC001460.

Teixell, A., P. Ayarza, H. Zeyen, M. Fernandez, and M.-L. Arboleya (2005), Effects of mantle upwelling in a compressional setting: The Atlas Mountains of Morocco, *Terra Nova*, *17*(5), 456–461, doi:10.1111/j.1365-3121.2005.00633.x.

Teixell, A., G. Bertotti, D. Frizon de Lamotte, and M. Charroud (2009), The geology of vertical movements of the lithosphere: An overview, *Tectonophysics*, *475*(1), 1–8, doi:10.1016/j.tecto.2009.08.018.

Thurner, S., I. Palomeras, A. Levander, R. Carbonell, and C.-T. Lee (2014), Ongoing lithospheric removal in the western Mediterranean: Evidence from Ps receiver functions and thermobarometry of Neogene basalts (PICASSO project), *Geochem. Geophys. Geosyst.*, *15*, 1113–1127, doi:10.1002/2013GC005124.

van Hunen, J., S. Zhong, N. Shapiro, and M. Ritzwoller (2005), New evidence for dislocation creep from 3-D geodynamic modeling of the Pacific upper mantle structure, *Earth Planet. Sci. Lett.*, *238*(1-2), 146–155, doi:10.1016/j.epsl.2005.07.006.

van Wijk, J. W., W. S. Baldridge, J. van Hunen, S. Goes, R. Aster, D. D. Coblentz, S. P. Grand, and J. Ni (2010), Small-scale convection at the edge of the Colorado Plateau: Implications for topography, magmatism, and evolution of Proterozoic lithosphere, *Geology*, *38*(7), 611–614, doi:10.1130/G31031.1.

Wagner, C., A. Mokhtari, E. Deloule, and F. Chabaux (2003), Carbonatite and Alkaline Magmatism in Taourirt (Morocco): Petrological, Geochemical and Sr-Nd Isotope Characteristics, *J. Petrol.*, *44*(5), 937–965.

Zhong, S., M. T. Zuber, L. Moresi, and M. Gurnis (2000), Role of temperature-dependent viscosity and surface plates in spherical shell models of mantle convection, *J. Geophys. Res.*, *105*(B5), 11,063–11,082.

